Criteria for Analysis of Multicomponent Tissue T_2 Relaxation Data

Simon J. Graham, Ph.D., Peter L. Stanchev, Ph.D., Michael J. Bronskill, Ph.D.

Monte Carlo simulations were performed to determine whether the multicomponent T_2 distribution of tissue can be estimated accurately from T_2 decay data acquired *in vivo*. Simulated data were generated for white matter, fast twitch muscle, and breast tissue. The signal-to-noise ratio, number of data samples, and minimum echo time were varied from the experimental conditions currently achievable with MRI to those achievable for *in vitro* experiments. Data were fitted by a distribution of T_2 values using the T2NNLS algorithm, and statistics characterizing the estimated T_2 components were determined. Current MRI techniques were found to provide conditions insufficient for accurate multicomponent T_2 analysis on a pixel-by-pixel basis. However, volume localization methods that measure T_2 decay from a large volume of interest have potential for this analysis. These results illustrate a general framework for development of new techniques to measure T_2 decay accurately *in vivo*.

Key words: T_2; relaxation time distributions; *in vivo* relaxometry; Monte Carlo simulations.

INTRODUCTION

Numerous studies of the magnetic resonance (MR) relaxation properties of tissues indicate that the T_2 decay of tissues is poorly represented by a single exponential. Most tissues exhibit several T_2 components in the range from 1 to 1000 ms that contribute different fractions, or weightings, to the net T_2 decay. Precise reasons why specific tissues exhibit multiple T_2 components remain unknown, although they are related to diffusive or other exchange processes between or within microscopic heterogeneous water environments in tissues. Knowledge of the multiple relaxation components that characterize tissue T_2 decay has direct application to optimization of MR imaging protocols (1). In addition, accurate multicomponent T_2 relaxation analysis is beginning to provide tissue-specific information in some applications, despite past literature reviews suggesting that tissue T_1 and T_2 values are not diagnostic (2).

Several examples illustrate the capabilities and potential applications of multicomponent T_2 relaxation analysis. Studies of excised tissues have shown that fast and slow twitch muscle can be distinguished by their respective T_2 distributions, for investigation of neurogenic and myogenic disease (3), and that the short T_2 component of white matter at 10 to 20 ms may be an indicator of multiple sclerosis (4). This analysis of white matter is being applied *in vivo* using imaging methods for spatial localization (5). T_2 relaxation properties of breast tissue, measured *in vivo* from a volume encompassing both breasts, correlate with x-ray mammographic parameters known to be a strong risk factor for breast cancer (6).

To exploit such findings clinically or in further research, accurate multicomponent T_2 analysis must be possible from data measured *in vivo* using MR scanners. Acquisition of such data carries its own set of challenges but we assume here that accurate relaxation data free from systematic errors can be obtained. (The following methodology also applies to data that are obtained with good precision but have known systematic errors, e.g., stimulated echo contamination. Usage of precise data often depends on the clinical context, whereas accurate data have wider applicability.) Fitting such decay data to resolve multiple T_2 components is itself a difficult inverse problem that places additional stringent requirements on the experimental conditions. Three parameters are sufficient to characterize the experimental conditions, or the quality of the T_2 decay data: the echo time, TE, the number of data samples, N, spanning the decay curve, and the signal-to-noise ratio (SNR). Magnetic resonance spectrometers modified for relaxometry can acquire high quality T_2 decay data with $TE \leq 1$ ms, $N > 100$, and SNR > 1000. By comparison, current T_2-weighted imaging protocols provide data (minimum $TE \cong 10$ ms, $N = 4-8$, pixel SNR $\cong 100$) that yield poor estimates of MR relaxation parameters. Intermediate between these two extremes, sets of experimental requirements for accurate multicomponent T_2 analysis exist that have not been fully assessed. These requirements probably depend both on specific T_2 characteristics of the tissue measured, and on the nature of the multicomponent T_2 relaxation analysis performed.

Investigation of experimental requirements for accurate multicomponent T_2 relaxation analysis provides a basis for the design of new MR techniques to measure T_2 decay *in vivo* with sufficient spatial localization. The alternatives for providing spatial localization are analogous to those for *in vivo* MR spectroscopy applications, where sufficient SNR is required to detect tissue metabolites present at low concentration (~1 mM) in realistic acquisition times. Either the MR spectrum of tissues can be mapped spatially, as in chemical shift imaging (CSI) methods (7), or the spectrum can be determined from a single volume of interest (VOI), as in single voxel volume localization methods (8). When CSI is used, spatial lo-

MRM 35:370–378 (1996)

From the Sunnybrook Health Science Centre and Department of Medical Biophysics, University of Toronto, Ontario, Canada.

Address correspondence to: Simon J. Graham, Ph.D., Imaging Research, Sunnybrook Health Science Centre, 2075 Bayview Avenue, Toronto, Ontario, Canada M4N 3M5.

Received February 15, 1995; revised August 10, 1995; accepted September 21, 1995.

This work was supported by a Terry Fox Programme Project grant from the National Cancer Institute of Canada, and General Electric Medical Systems, Canada.

Present address (P.L.S.): Institute of Mathematics, Bulgarian Academy of Sciences, Academy G, Sofia, Bulgaria.

0740-3194/96 $3.00

Copyright © 1996 by Williams & Wilkins
All rights of reproduction in any form reserved.

calization is obtained typically by slice-selective excitation and phase encoding in two dimensions; when volume localization is used, a VOI is isolated in three spatial dimensions using selective RF pulses, without phase encoding. Volume localization thus allows acquisition of MR spectra with full T_1 recovery in times much shorter than is possible with CSI. For example, proton MR spectra with sufficient SNR can be obtained typically in <10 min with volume localization, whereas CSI requires acquisition times of approximately 30 minutes (9, 10). The gain in SNR per unit time provided by volume localization is, however, achieved at the expense of spatial resolution and volume of coverage. The choice of method for spatial localization therefore depends on the particular application.

Both imaging and volume localization techniques have been developed for quantitative measurement of T_2 decay *in vivo*. Spin-echo imaging pulse sequences for measurement of T_2 decay in a single slice have been developed (5, 11) that are robust to experimental imperfections and increase N to 32, but maintain minimum TE and pixel SNR similar to T_2-weighted imaging described above. Subsequent references to imaging methods are made with respect to these robust techniques, unless otherwise stated. Alternatively, a volume localization method has recently been developed to measure multicomponent T_2 decay of breast tissue with a minimum TE of 2.5 ms, $N = 70$, and SNR = 700, for a VOI comprising approximately 50% of the total breast volume (6).

In this study, Monte Carlo simulations are used to investigate data requirements for multicomponent T_2 relaxation analysis under the experimental conditions common to clinical MR scanners. Data sets are generated by adding noise to signals calculated from well determined T_2 distributions. The non-negative least squares algorithm modified by Whittall *et al.* (T2NNLS), frequently used in analysis of multicomponent T_2 tissue relaxation (3, 4, 6, 12), provides a constrained fit to the simulated T_2 decay data sets with a smooth distribution of relaxation times (13). Three groups of simulations are performed. First, two variations of multicomponent T_2 analysis using T2NNLS are compared to determine which is more appropriate under the conditions of low SNR typical for *in vivo* data. Second, representative tissues well characterized by previous relaxation measurements *in vitro* are analyzed, with emphasis on the features of their T_2 distributions that are important for clinical applications. The data quality necessary for accurate estimation of these features is determined and compared with that achievable using imaging methods. Third, multicomponent T_2 analysis of breast tissue is assessed and compared to data obtained *in vivo* with volume localization (6). This comparison determines the relative contributions of statistical uncertainty and biological variability in the T_2 distributions. These simulations are shown to provide a general framework for assessing whether multicomponent T_2 relaxation analysis of *in vivo* data is feasible in specific applications.

METHODS

Simulation of T_2 Data

From the literature, nominal T_2 values and relative weightings were obtained for T_2 components of white matter, fast twitch muscle, and slow twitch muscle at 1.5 T (4, 3), shown in Table 1. These tissues have been carefully characterized *in vitro* and the distribution parameters are assumed to reflect the true T_2 distributions of these tissues accurately.

Simulated T_2 decay data were generated from

$$y_n = y_o \sum_{j=1}^{J} \int D_j(T_2) e^{-(n\,TE/T_2)} dT_2 + \epsilon(0, \sigma), \qquad [1]$$

where y_n represents signal amplitude measured at time intervals TE with $n = 1,2, \ldots, N$; y_o represents the initial amplitude of the signal (arbitrarily set at 100); the subscript j represents each relaxation component (J components in total), and $D_j(T_2)$ is the piecewise continuous portion of the T_2 distribution associated with component j. Because tissue T_2 decay is not well represented by a weighted sum of several exponentials (14), components were assumed to follow a Gaussian distribution with mean T_2 value T_{2_j}, fractional weighting w_j, and standard deviation equal to 10% of T_{2_j}, and were truncated to zero for T_2 values greater than four standard deviations from T_{2_j}. Component widths of 10% were chosen to provide a realistic test of the methodology, because the width of each relaxation component in Table 1 has not yet been reliably determined by experiment. The term $\epsilon(0, \sigma)$ indicates the addition to each datum of zero mean, Gaussian random noise of standard deviation σ. To simulate the broad range of measurement conditions possible *in vivo*, the SNR value, defined as M_o/σ, and N were varied in the range from 100 to 2000, and 32 to 256, respectively. For each set of experimental parameters, 200 trials were performed from which the statistical accuracy of multicomponent T_2 relaxation analysis was determined.

Fitting of T_2 Data

The simulated data were fitted by a distribution of T_2 values using the T2NNLS algorithm (13, 15) based on the non-negative least squares (NNLS) algorithm of Lawson

Table 1
Nominal T_2 Distribution Parameters at 1.5 T for Tissues Used in Simulations

Tissue	T_{2_1} (ms)	T_{2_2} (ms)	T_{2_3} (ms)	w_1 (%)	w_2 (%)	w_3 (%)
White matter	15	100	—	10	90	—
Muscle (fast twitch)	5	33	115	5	90	5
Muscle (slow twitch)	5	35	115	5	85	10

and Hanson (16). With this analysis, the T_2 decay data are represented by a system of discrete linear equations:

$$\tilde{y}_n = \sum_{m=1}^{M} S_m e^{-(n\,TE/T_{2_m})}, \quad [2]$$

where S_m is the estimated amplitude of the T_2 distribution (the number of protons with a particular T_2 value) at position T_{2_m}, and $e^{-(nTE/T_{2_m})}$ is the associated exponential decay for each T_{2_m}. The S_m values are constrained to be non-negative (i.e., positive) as a direct result of the NNLS algorithm. To span the T_2 values of the distributions in Table 1 appropriately, 50 T_{2_m} values were chosen equally spaced on a logarithmic scale, extending from a lower limit of 1 ms to an upper limit several hundred milliseconds above the largest T_2 component value for each specific tissue. An additional large T_2 value ($10 \cdot T_{2_{50}}$) was included, for which the exponential term in Eq. [2] was approximately unity, thus, the corresponding S_{51} value provided an estimate of constant baseline offset.

The S_m, and thus $\tilde{y}_n$, values are determined by minimization of

$$\sum_{n=1}^{N} \frac{(y_n - \tilde{y}_n)^2}{\sigma_n^2} + \frac{1}{\mu} f(S_1, S_2, \cdots, S_M). \quad [3]$$

The first term provides the standard least squares minimization common to many fitting algorithms. The presence of noise, however, ensures that there are a large number of T_2 distributions that satisfy Eq. [3] within experimental error. For example, Brown has investigated the difficulty involved in distinguishing continuous T_2 distributions from distributions corresponding to a small number of discrete exponentials (17). The approach adopted here is to restrict the set of T_2 distributions according to the "principle of parsimony," which requires that the most appropriate solutions are the simplest ones, i.e., those that are least complex. The second term in Eq. [3], known as a regularizer, provides additional constraint to ensure a parsimonious set of T_2 distributions.

In this study, the regularizer was chosen as the energy of the T_2 distribution:

$$f(S_1, S_2, \cdots, S_M) = \sum_{m=1}^{M} S_m^2. \quad [4]$$

When the energy of the T_2 distribution is minimized together with the least squares misfit, smooth, low amplitude T_2 distributions are obtained. These "minimum energy constraints" have been applied previously (13) and provide estimated T_2 distributions similar to those produced by other regularizer functions, such as first or second derivative constraints (13, 14).

The strength of regularization in Eq. [3] depends on the value chosen for the constant μ. Very large μ values reduce the constraints, and in the limit result in a conventional unregularized least squares fit producing a T_2 distribution that consists of delta functions. Very small μ values produce broad, overconstrained distributions. Some strategy is therefore required to choose an appropriate intermediate value. Previously, Whittall and MacKay (13) have selected μ according to the χ^2 misfit:

$$\chi^2 = \sum_{n=1}^{N} \frac{(y_n - \tilde{y}_n)^2}{\sigma^2}, \quad [5]$$

i.e., the first term in Eq. [3]. For large N, the expected value of χ^2 is N, corresponding to an acceptable fit where the difference between each measured and estimated datum, $y_n - \tilde{y}_n$, is the standard deviation of the noise, σ. The standard deviation of χ^2, however, is approximately $\sqrt{2N}$ and so distributions that result in χ^2 misfits approximately 1 standard deviation from N can all be considered acceptable. Unacceptable fits have $\chi^2 \gg N$, indicating that the fitted curve does not follow the data, or have $\chi^2 \ll N$, indicating that the fitted curve follows the data too well and is strongly influenced by noise. The latter case is typical of T_2 decay data (13). Therefore, a logical strategy is to choose μ such that

$$\chi^2 = N + x\sqrt{2N} \quad [6]$$

for all fits, with $0 \leq x \leq 1$. For this "constant χ^2 constraint," T_2 distributions obtained from different data sets can be compared effectively because they all have the same χ^2 misfit. In practice, this procedure necessitates multiple applications of T2NNLS to the same data set while adjusting μ iteratively until Eq. [6] is satisfied, and any data sets producing an unregularized χ^2 misfit larger than Eq. [6] are rejected.

Constant χ^2 constraints are only one of many possible strategies for choosing μ, and in particular, may not be optimal for the reduced data quality that is expected for *in vivo* T_2 decay data. Therefore, an alternative strategy, termed "least squares-based constraints," was also investigated that slightly regularizes all data sets equally on a percentage basis. Specifically, μ was iteratively adjusted such that

$$\chi^2 = \chi^2_{min} \frac{(100\% + y)}{100\%}, \quad [7]$$

where χ^2_{min} is the unregularized least squares misfit, and y is a constant that determines the percentage increase in χ^2 above χ^2_{min}. No solutions are rejected with this set of constraints. The range of useful y values was investigated empirically.

Analysis criteria

T_2 distributions obtained by both constraint methods were analyzed by calculating the T_2 value (first moment), relative weighting, and width (second moment) of each component, and $<T_2>$, the mean T_2 (first moment) of the entire distribution. Estimated components below specific threshold T_2 and weighting values for each tissue were labeled "spurious," and were ignored, to eliminate the dependence of the fits to the initial T_2 decay samples, and to remove any estimated T_2 components largely hidden within the T_2 decay noise envelope. Overlapping components were judged to be adequately resolved when the minimum between components was <70% of the

amplitude of the smaller component. For each set of 200 trials representing a specific set of experimental conditions, the "admissibility" (percentage of distributions with the correct number of components) was calculated, as well as the mean and standard deviation of each parameter estimated from the T_2 distribution.

The two strategies for applying constraints were initially compared by performing three tasks: a) assessment of admissibility for white matter under conditions of fixed N and TE, for varying SNR; b) assessment of the SNR required to resolve two components with T_{2_j} values separated by a factor of three; c) assessment of the width of a single T_2 component for fixed N and TE, and for varying SNR. Results favored the least squares-based constraint with $y = 1\%$, which was used at low values of SNR and N.

For white matter, fast twitch, and slow twitch muscle simulations, SNR was varied for different values of N and TE, to assess the level required to determine T_2 distribution parameters within a specific tolerance (typically a standard deviation of <10%). The component of white matter with $T_2 = 15$ ms may reflect the water associated with the myelin sheath of neurons, and decreased weighting of this component has been correlated with demyelination (4). Simulations were therefore performed to determine the SNR required to estimate the weighting of this component accurately, as well as the optimum echo time, TE_{opt}, for a range of different N values. For fast and slow twitch muscle, distinguishing the two tissues is of interest. From Table 1, the first moments of the T_2 distributions for fast and slow twitch muscle are 35.7 ms and 41.5 ms respectively. Therefore, the SNR required to estimate $<T_2>$ within 1 ms was determined for various conditions.

Simulation of *in vivo* measurements of breast tissue

Simulations were also performed to investigate further the T_2 distribution parameters of breast tissue obtained from measurements of female volunteers using volume localization, acquired in 40 s (6). This methodology, designed to address whether MR measurements can be used to assess risk of breast cancer, has not focused in detail on the T_2 distribution of breast tissue. The T_2 distribution reflects biophysical properties of tissue related to the dynamics of water and fat molecules, and potentially contains additional information to improve risk assessment. Previous measurements have indicated that the mean value of the T_2 distribution shows significant variations over the wide range of breast tissue characteristics found in women (6), but analogous variations could not be detected for specific component T_2 values and weightings within the T_2 distribution. These results are initially counterintuitive. Simulations were performed, therefore, to determine the variation in the estimated T_2 parameters arising solely from errors in multicomponent T_2 relaxation analysis, under conditions closely approximating those of the actual measurements *in vivo*.

Shown in Table 2 are the mean and standard deviation of the three T_2 components of breast tissue obtained by volume localization in 29 of the 38 female subjects (6). (Of the other nine subjects, seven exhibited two T_2 components, and two exhibited four T_2 components.) Simulated T_2 decay data were generated and analyzed as described previously, using the values in Table 2, and the same TE and number of data samples used in the actual experiments ($TE = 16$ ms, $N = 70$). Component widths of 10% were assumed. A wide range of SNR values was chosen based on the actual distribution of SNR values for the volunteers shown in Table 3. Wide variations in torso size of the volunteers, and the large sensitive volume of the surface coil, are responsible for this range of SNR values. Because the uncertainty in estimating T_2 distribution parameters is largest at low SNR values, Table 3 is shown with unequal SNR intervals, with the interval size increasing as SNR increases. These intervals provide acceptable local averages of the uncertainty in estimating T_2 parameters with T2NNLS. The mean and standard deviation of the T_2 distribution parameters were evaluated for the SNR values shown in the middle column, combined according to the frequency distribution, and compared with the estimates obtained from the actual data.

Table 2
Three T_2 Components Obtained in 29 of 38 Volunteers

Parameter	Mean	Standard deviation
T_{2_1} (ms)	34	12
T_{2_2} (ms)	105	29
T_{2_3} (ms)	340	114
w_1 (%)	25	11
w_2 (%)	55	9
w_3 (%)	20	12

RESULTS

Comparison of Constraint Strategies

Figure 1 shows admissibility versus SNR for white matter for different applications of constant χ^2 and least-squares based constraints ($N = 64$, $TE = 3.5$ ms). All estimated components with $T_2 < 8$ ms or weighting <3% were ignored. Admissibility for the unconstrained least squares fit ($y = 0$) is highest at SNR = 100, but progressively overestimates the true number of components for increasing SNR values. At SNR = 1000, the admissibility of unconstrained fits has decreased to 75%. Admissibility for least squares-based constraints, however, is >90% over the entire SNR range and is only weakly dependent on the chosen value of y. Admissibility for all constant χ^2 constraints starts at approximately 25% for SNR = 100,

Table 3
Frequency Distribution of SNR for Breast Tissue Measurements of 38 Volunteers

SNR Interval	SNR Evaluated	Frequency
0–174	100	6
175–374	250	5
375–674	500	10
675–874	750	3
875–1249	1000	7
1250–1749	1500	3
1750–3000	2000	4

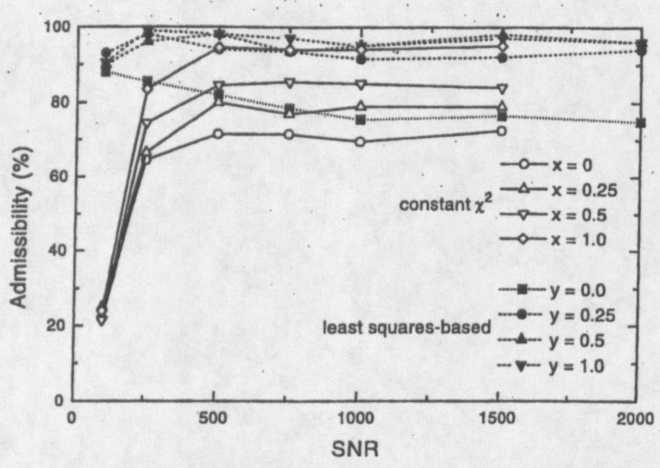

FIG. 1. Admissibility versus SNR for constant χ^2 constraints ($0 \leq x \leq 1$) and least squares-based constraints ($0 \leq y \leq 1\%$). The unconstrained, least squares fit is shown with $y = 0$.

and increases to a constant value for SNR > 500 that depends strongly on x. Of the x values chosen, an admissibility of >90% only occurs for $x = 1.0$. Slightly larger x values (e.g., $x = 1.5$) provide a slight gain in admissibility at low SNR values, but with increased bias in estimated distribution parameters (data not shown).

Figure 2 shows the SNR required by each constraint strategy to resolve two components with T_2 values separated by a factor of three, with an admissibility >90%, and <10% uncertainty in T_2 and weighting estimates. The T_2 values were 33 and 100 ms, respectively, w_1 varied from 10% to 90%, N varied from 32 to 128, and $N \cdot TE$ was held fixed at 650 ms to maintain uniform sampling of the simulated T_2 decay. All estimated components with $T_2 < 15$ ms were ignored. Constant χ^2 constraints were applied with $x = 1.0$, and least squares-based constraints with $y = 1.0\%$. Each threshold curve exhibits a minimum for $w_a \cong 50\%$, indicating that equally weighted components are easier to resolve than if one component dominates. For both constraint strategies, a logarithmic dependence between N and SNR is indicated by the constant shift upward of the threshold curves on the semi-logarithmic plot, as N decreases by factors of 2. Most importantly, however, the observed thresholds for least squares-based constraints are almost always lower than for those for constant χ^2 constraints.

Figure 3 shows width estimates of one simulated component ($T_2 = 100$ ms) versus SNR for both constraints. Component widths of 10% and 20% were investigated with $N = 64$, and TE values of 10 ms and 20 ms, respectively, to span the same range of decay in both cases. For constant χ^2 constraints, width is greatly overestimated at low SNR values but tends asymptotically to the correct value as SNR increases. Least squares constraints provide mean estimates much closer to the true width for all SNR values.

Because of their superior characteristics at low values of SNR and N, least squares-based constraints were utilized for all subsequent analysis.

White Matter

Figure 4 shows the SNR required to estimate w_1 for white matter (admissibility >90%, deviation of w_1 <10% from the value in Table 1) as a function of TE for N ranging from 32 to 256. Spurious components were ignored as for the analysis shown in Fig. 1, and $y = 1.0\%$. For each N, there is an optimal TE value, TE_{opt}, that provides the minimum SNR. For $TE < TE_{opt}$, the component of white matter at $T_2 = 100$ ms is undersampled, whereas for $TE > TE_{opt}$, the component at $T_2 = 15$ ms is undersampled. Log-log plots of the minimum SNR and TE_{opt} versus N are shown in Fig. 5, which suggest that both parameters can be described as a function of N according to

$$a \cdot N^b = 10^c, \qquad [8]$$

where a represents the SNR or TE_{opt} values, and b and c are constants. The solid lines in Fig. 5 indicate fits of SNR and TE_{opt} to this relationship. For SNR data, $b = 0.56 \pm 0.04$ and $c = 3.50 \pm 0.08$ ($P < 0.01$), and for TE_{opt} data, $b = 0.76 \pm 0.07$ and $c = 1.95 \pm 0.13$ ($P < 0.01$).

Distinguishing fast from slow twitch muscle

Multicomponent T_2 analysis to distinguish fast from slow twitch muscle is at first glance more difficult than analysis of white matter. Both T_2 distributions of muscle

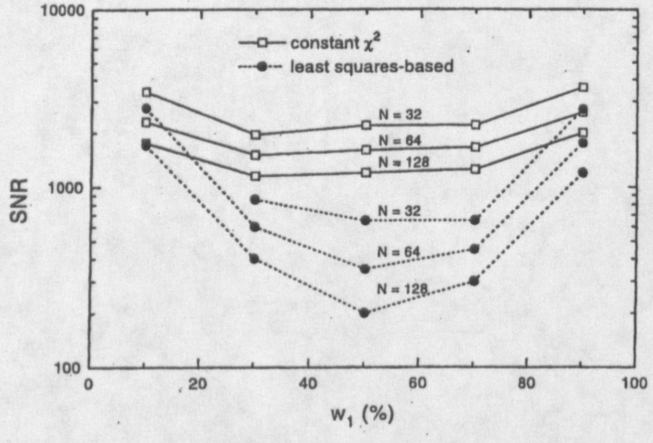

FIG. 2. SNR for resolving a two component distribution versus w_1 for both constraint strategies. Data were determined with an SNR accuracy of ±50.

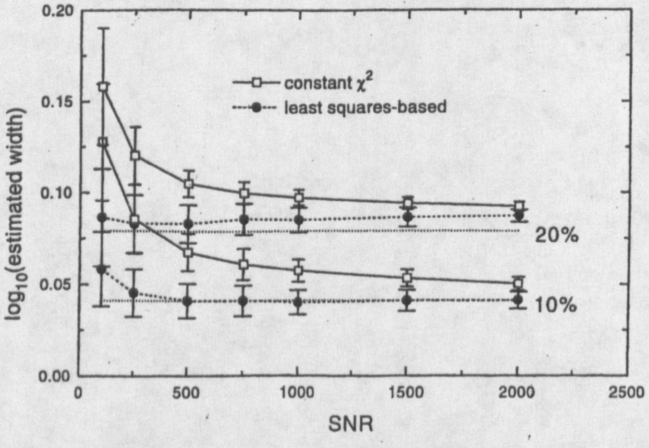

FIG. 3. Estimated width of a single component T_2 distribution versus SNR for both constraint strategies. Model widths of 10% and 20% are shown. Error bars indicate the standard deviation of width estimates from 200 trials.

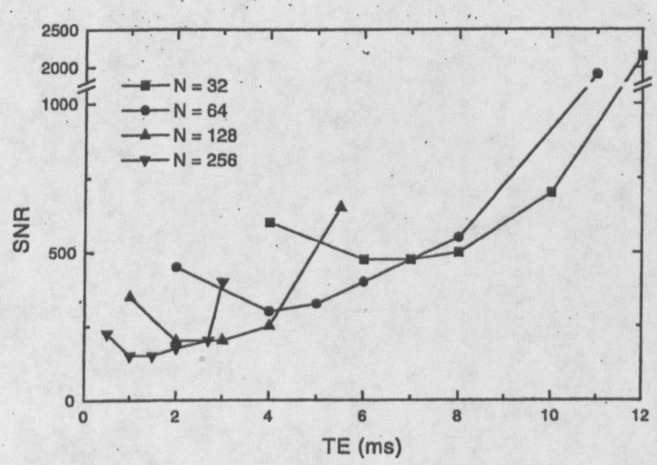

FIG. 4. SNR required to estimate w_1 versus *TE* for white matter (admissibility >90%, standard deviation <10%). The SNR was determined to within ±50 for each datum.

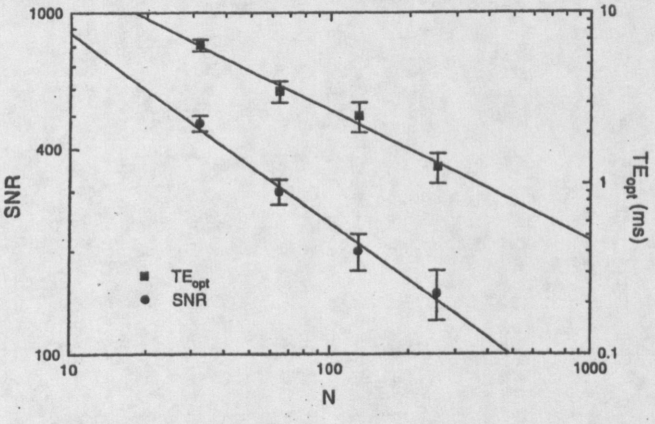

FIG. 5. Log–log plots of SNR versus *N* and TE_{opt} versus *N* for white matter. Error bars indicate the uncertainty with which SNR and TE_{opt} were determined from Fig. 4.

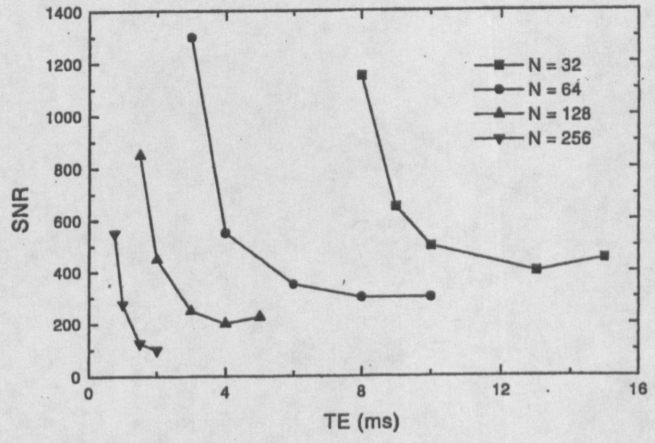

FIG. 6. SNR versus *TE* for estimation of $<T_2>$ to an accuracy of 1 ms for fast twitch muscle. The SNR was determined to within ± 25 for each datum.

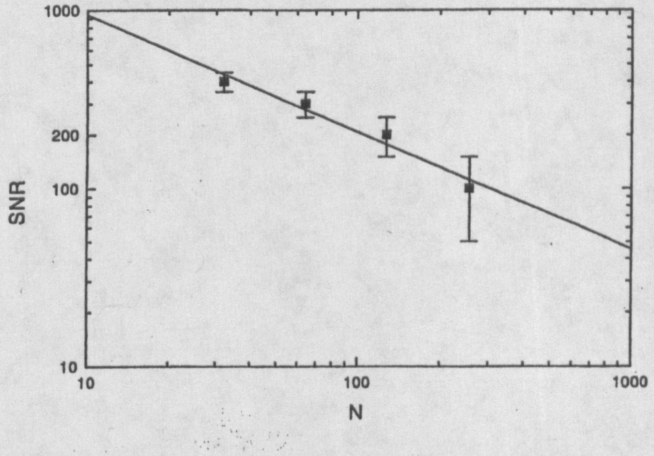

FIG. 7. SNR versus *N* for fast twitch muscle. Error bars indicate the accuracy with which the minimum SNR was determined from Fig. 6.

exhibit three relaxation components. Accurate determination of the component with $T_2 = 5$ ms requires a small *TE* value, necessitating data sampling with large *N* to resolve the other two components with acceptable admissibility. For example, for $N = 256$, $TE_{opt} = 1.75$ ms and the minimum SNR is 450, or three times the analogous value for white matter. In this application, however, the first moment of the distribution, $<T_2>$, provides more robust analysis. The T_2 distributions of slow and fast twitch muscle differ primarily in the position and weighting of the two components with $T_2 > 5$ ms. Poor sampling of the short T_2 component causes only a small offset in $<T_2>$ that tracks similarly for both muscle types.

Figure 6 shows the SNR for fast twitch muscle versus *TE* for different values of *N*. The $<T_2>$ accuracy required was 1 ms. (Analysis of fast twitch muscle is more difficult because the component weighting w_3 is smaller than for slow twitch muscle. Therefore, the $<T_2>$ accuracy for analysis of slow twitch muscle can be assumed as ≤ 1 ms.) Components with $T_2 < 2.5$ ms were ignored, and $y = 0.5\%$. Figure 6 indicates ranges of *TE* values that produce similar minimum SNR values for determining $<T_2>$ accurately, because precise determination of the short T_2 component is not required. The dependence of the SNR value on *N* can again be represented by Eq. [8], as shown in Fig. 7. In this case, the fitted parameters for SNR are $b = 0.65 \pm 0.09$ and $c = 3.6 \pm 0.2$ ($P < 0.02$).

Breast tissue

The estimated T_2 components for breast tissue, determined by simulation of the actual experimental conditions ($TE = 16$ ms, $N = 70$), are shown in Table 4. The simulation results are close to those obtained from the actual experimental data (Table 2). It was found that the mean admissibility estimate was sensitive to the precise details of the SNR frequency distribution (Table 3). The quoted value for admissibility in 200 trials (70 ± 5%) therefore represents the mean, and maximum deviation from the mean, obtained by performing several calculations with different bin sizes for the SNR frequency distribution. The simulation estimate agrees well with the value of 76% obtained experimentally, representing a difference in classification of 2 ± 3 individuals in 38. All other parameters were quite insensitive to the bin size of the SNR frequency distribution, and therefore error estimates are not given. The mean T_2 distribution parameters estimated by simulation and experiment agree to well within the standard deviations indicated. The largest

Table 4
T_2 Distribution Parameters of Breast Tissue Estimated by Monte Carlo Simulation

Parameter	Mean	Standard deviation
admissibility (%)	70 ± 5	—
T_{2_1} (ms)	30	6
T_{2_2} (ms)	102	10
T_{2_3} (ms)	344	33
w_1 (%)	22	5
w_2 (%)	59	4
w_3 (%)	19	3

discrepancy occurs for estimation of T_{2_1} and w_1. The standard deviations of the T_2 distribution parameters, however, are less than those obtained for the experimental data by a factor of 2 to 4.

DISCUSSION

In the past, simulation studies have been performed to assess the accuracy of multicomponent T_2 relaxation analysis for T2NNLS (13, 15, 18), and another algorithm, CONTIN (14, 19, 20), for arbitrary T_2 distributions under the experimental conditions typical of *in vitro* experiments. English *et al.* also used simulations to validate their multicomponent T_2 analysis of fast and slow twitch muscle data acquired *in vitro* (3). We have developed a general extension of this methodology for multicomponent T_2 relaxation analysis of *in vivo* data. The applicability of this analysis, either clinically or in biophysical research, depends on the specific multicomponent T_2 properties of tissues and the manner in which the estimated T_2 distribution is analyzed, both of which are invariably investigated initially by *in vitro* experiments with the best data quality available. The information obtained from previous *in vitro* measurements can be used in Monte Carlo simulations to investigate how specific T_2 data can be measured *in vivo*, analyzed, and interpreted, appropriately. We have used representative examples to investigate each of these issues.

Simulations were first conducted to compare the suitability of different constraint strategies for multicomponent T_2 relaxation analysis of *in vivo* data using T2NNLS. Figures 1–3 indicate that constant χ^2 constraints, often used for multicomponent T_2 relaxation analysis at high values of SNR and N (SNR > 1000, $N > 100$), are suboptimal for the poorer experimental conditions typical of *in vivo* data. At intermediate to low SNR values, least squares-based constraints provide enhanced admissibility and allow lower SNR for estimating T_2 components within a specified accuracy. Also, any systematic T_2 offset in component estimates is generally less with least squares-based constraints than with constant χ^2 constraints (data not shown).

To date, least squares-based constraints have not been commonly applied. At extremely low SNR values, other investigators have opted for the enhanced admissibility provided by unregularized least squares fits (see Fig. 1). For example, MacKay *et al.* used unregularized fits to estimate the *in vivo* T_2 distribution of white matter for volunteers with multiple sclerosis (5). The simulations indicate that for low SNR values, the addition of minimum energy constraints to increase χ^2 by only a small amount (≤1%) above χ^2_{min} can provide admissibilities >90% and decrease the uncertainty in component estimates. Least squares-based constraints also improve the ability to estimate the width of T_2 components, which may be useful for investigation of subtle variations in the T_2 distributions of white and gray matter in different regions of the brain (21).

Analyses of simulated T_2 decay for white matter and fast twitch muscle were performed with least squares-based constraints to determine whether current imaging techniques generate data of sufficient quality for accurate multicomponent T_2 analysis. In both cases, imaging techniques were found to provide sufficient data quality only for long scan times. Typical imaging parameters are a minimum *TE* of 10 ms, $N = 32$, and a pixel SNR of 100 (11). For analysis of the short T_2 component of white matter with $N = 32$ (Figs. 4 and 5), *TE* of 10 ms is significantly larger than the TE_{opt} of 6.5 ms, and the required SNR would be 700. If the time to acquire one image is approximately 2 min (128 phase encoding steps × 1 *s TR*), signal averaging to achieve this SNR would require a total scan time of 98 min, which is not clinically feasible. A similar calculation for distinguishing fast from slow twitch muscle using $<T_2>$ still requires a total scan time of 32 min, which is long but more practical.

The dependence of SNR on N is well described by a straight line on a log-log plot. This result was observed for both estimation of the weighting of a single component in the T_2 distribution of white matter, and estimation of $<T_2>$ for fast twitch muscle. Similar observations have been made in other studies; Whittall *et al.* (15) observed that the ability to resolve T_2 components using the method of Backus and Gilbert (22) was characterized by

$$SNR \cdot N^{1/2} = const, \quad [9]$$

when T_2 decay data samples are acquired at logarithmic time intervals. For white matter, the fitted exponent of N (Fig. 5) shows a similar dependence ($b = 0.56 \pm 0.04$), whereas for fast twitch muscle (Fig. 7), the exponent is somewhat higher ($b = 0.65 \pm 0.09$). When experimental error is considered, however, the fitted exponents for white matter and fast twitch muscle are not significantly different, and a slightly larger value than $b = 0.5$ may reflect the difference between logarithmic data sampling versus linear data sampling used in this study.

Equation [9] can also be used to interpret multicomponent T_2 relaxation analysis more generally. In Fig. 8, results of the simulations for white matter and fast twitch muscle have been replotted with $SNR \cdot N^{1/2}$ as the vertical axis, and the total sampling interval $N \cdot TE$ as the horizontal axis. The square root dependence of SNR minimum on N, as observed in Figs. 4–7, is therefore removed so that additional features of the data can be interpreted. All data sets with different N values in Figs. 8a and 8b follow a sharply decreasing trend for increasing total sampling interval (solid line) starting from large values of $SNR \cdot N^{1/2}$, reflecting poor data sampling of the relaxation components with comparatively large T_2 val-

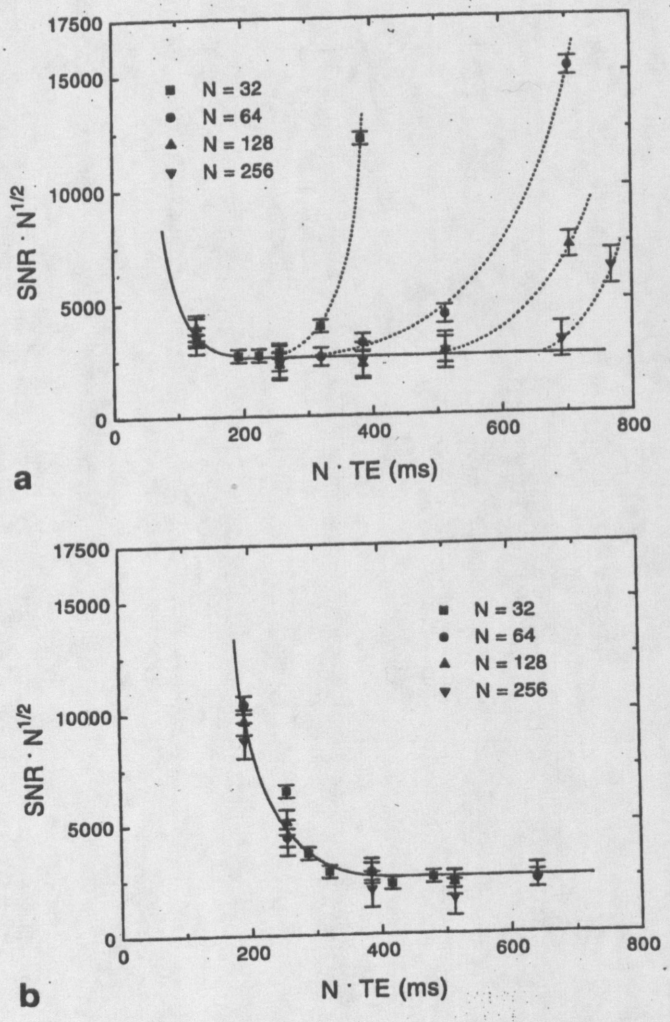

FIG. 8. Data for (a) white matter and (b) fast twitch muscle replotted with SNR · $N^{1/2}$ as the vertical axis and $N \cdot TE$ as the horizontal axis. Solid and dashed lines indicate trends.

ues, toward a minimum SNR · $N^{1/2}$ value of approximately 2500, which is apparently an intrinsic threshold for these analyses. Because the specified analysis of fast twitch muscle requires accurate estimation of a component with $T_2 = 115$ ms, whereas the component of interest for white matter has $T_2 = 15$ ms, the data in Fig. 8b are shifted to the right when compared to those in Fig. 8a. For fast twitch muscle, all data sets follow the same relationship independent of N over the range of total sampling intervals shown, and optimal results require only that the total sampling interval be sufficiently large (i.e., >300 ms) to sample the component with $T_2 = 115$ ms adequately. For white matter, SNR · $N^{1/2}$ reaches the minimum value and then increases as resolution of the component at $T_2 = 15$ ms is progressively lost (dashed lines), such that there is actually a range of acceptable sampling intervals for each N. As N increases, the range of acceptable sampling intervals also increases; usage of a specific TE_{opt} value becomes less important. For very large N, any TE value can be chosen as long as the component at $T_2 = 15$ ms is adequately sampled.

The third set of simulations, performed for breast tissue, illustrate how the methodology can be used to validate and interpret multicomponent T_2 relaxation analysis of *in vivo* data. For the experimental conditions actually obtained using volume localization (6), the mean parameter estimates of the T_2 distribution for simulated and measured data agree, suggesting that the SNR and data sampling obtained with volume localization are sufficient to resolve these three T_2 components on average. Variation in parameter estimates is larger for the measured data, consistent with the wide variation in breast tissue characteristics typically observed for volunteer subjects (23), although the variation observed for the simulated data suggests that increased SNR is required to measure biological variations in individual T_2 components of breast tissue accurately *in vivo*.

We are currently undertaking an *in vitro* study to identify which features of the breast T_2 distribution correspond to fibroglandular and adipose tissue, to investigate how the distribution varies for different fibroglandular fractions, and to compare the results obtained with those presented here as well as with those of other investigators (24). Together with Monte Carlo simulations, *in vitro* measurements should provide valuable information for optimizing measurement of breast T_2 decay data *in vivo* for assessment of risk of breast cancer (6).

Simulations play an important role in assessing the suitability of different techniques for measuring T_2 decay with sufficient data quality and spatial localization *in vivo*. For measurement of breast tissue, the data quality from volume localization represents a marked improvement over that obtained by imaging methods. By comparison, Poon *et al.* were unable to detect significant differences in the mean T_2 value of a single, midbreast slice, for breasts with low and high fractions of fibroglandular tissue (25). Whether volume localization methods can be extended to other applications of multicomponent T_2 relaxation analysis remains a question. The gain in T_2 resolution provided by volume localization is achieved partly at the expense of spatial resolution. For a given application, the VOI size must provide sufficient localization that the relevant T_2 components are resolved without significant degradation in data quality. Further pulse sequences that meet these constraints remain to be developed for specific clinical applications.

CONCLUSION

Monte Carlo simulations indicate that least squares-based, rather than constant χ^2, constraints are preferable for multicomponent T_2 relaxation analysis of data with low SNR typical of *in vivo* measurements. Current MR imaging methods are insufficient to estimate accurately the T_2 distributions of white matter or slow and fast twitch muscle on a pixel-by-pixel basis to the tolerances specified, in sufficiently short scan times. The conditions of a previous study using volume localization were sufficient, however, to resolve the three T_2 components of breast tissue observed. This work provides a general framework for assessing the quality of T_2 decay data necessary for the development of new techniques to measure multiple T_2 components accurately *in vivo*.

REFERENCES

1. E. R. McVeigh, R. M. Henkelman, M. J. Bronskill, Optimization of survey protocols for MRI. *Magn. Reson. Med.* **13,** 177–191 (1990).
2. P. A. Bottomley, T. H. Foster, R. E. Argersinger, L. M. Pfeifer, A review of normal tissue hydrogen NMR relaxation times and relaxation mechanisms from 1–100 MHz: dependence on tissue type, NMR frequency, temperature, species, excision, and age. *Med. Phys.* **11,** 425–447 (1984).
3. A. E. English, M. L. G. Joy, R. M. Henkelman, Pulsed NMR relaxometry of striated muscle fibres. *Magn. Reson. Med.* **21,** 264–281 (1991).
4. W. A. Stewart, A. L. MacKay, K. P. Whittall, G. R. Wayne-Moore, D. W. Paty, Spin-spin relaxation in experimental allergic encephalomyelitis: analysis of CPMG data using a non-linear least squares method and linear inverse theory. *Magn. Reson. Med.* **31,** 767–775 (1993).
5. A. L. MacKay, K. P. Whittall, J. Adler, D. Li, D. W. Paty, D. Graeb, In vivo visualization of myelin water in brain by magnetic resonance. *Magn. Reson. Med.* **31,** 673–677 (1994).
6. S. J. Graham, M. J. Bronskill, J. W. Byng, M. J. Yaffe, N. F. Boyd, Quantitative correlation of breast tissue parameters using magnetic resonance and x-ray mammography. *Br. J. Cancer.* in press.
7. T. R. Brown, B. M. Kincaid, K. Ugurbil, NMR chemical shift imaging in three dimensions. *Proc. Natl. Acad. Sci. (USA)* **79,** 3523–3526 (1982).
8. R. J. Ordidge, M. R. Bendall, R. E. Gordon, A. Connelly, *in* "Magnetic Resonance in Biology and Medicine" (G. Govil, C. L. Khetrapal, A. Saran, Eds.), p. 387, Tata McGraw-Hill, New Delhi, 1985.
9. J. Frahm, W. Hanicke, *in* "Basic and Advanced Magnetic Resonance Spectroscopy Course Syllabus," p. 206, Society of Magnetic Resonance, Berkeley, 1994.
10. D. M. Spielman, J. M. Pauly, A. Macovski, G. H. Glover, D. R. Enzmann, Lipid-suppressed single- and multisection proton spectroscopic imaging of the human brain. *J. Magn. Reson. Imaging* **2,** 253–262 (1992).
11. C. S. Poon, R. M. Henkelman, Practical T2 quantitation for clinical applications. *J. Magn. Reson. Imaging.* **2,** 541–553 (1992).
12. R. S. Menon, M. S. Rusinko, P. S. Allen, Proton relaxation studies of water compartmentalization in a model neurological system. *Magn. Reson. Med.* **28,** 264–274 (1992).
13. K. P. Whittall, A. L. MacKay, Quantitative interpretation of NMR relaxation data. *J. Magn. Reson.* **84,** 134–152 (1989).
14. R. M. Kroeker, R. M. Henkelman, Analysis of biological NMR relaxation data with continuous distributions of relaxation times. *J. Magn. Reson.* **69,** 218–235 (1986).
15. K. P. Whittall, M. J. Bronskill, R. M. Henkelman, Investigation of analysis techniques for complicated NMR relaxation data. *J. Magn. Reson.* **95,** 221–234 (1991).
16. C. L. Lawson, R. J. Hanson, "Solving Least Squares Problems," Prentice-Hall, Inc., Englewood Cliffs, NJ, 1974.
17. R. J. S. Brown, Information available and unavailable from multiexponential relaxation data. *J. Magn. Reson.* **82,** 539–561 (1989).
18. F. R. E. Fenrich, P. S. Allen, A simulation evaluation of a linear inverse technique for determining continuous relaxation time distributions, *in* "Proc., SMRM, 11th Annual Meeting, Berlin, 1992," p. 1309.
19. S. W. Provencher, CONTIN: A general purpose constrained regularization program for inverting noisy linear algebraic and integral equations. *Comput. Phys. Commun.* **27,** 229–242 (1982).
20. S. W. Provencher, A Fourier method for analysis of exponential decay curves. *Biophys. J.* **16,** 27–41 (1976).
21. A. L. MacKay, K. P. Whittall, R. A. Nugent, D. Graeb, I. Lees, D. K. B. Li, In vivo T2 relaxation in normal human brain, *in* "Proc., SMR, 2nd Annual Meeting, San Francisco, 1994," p. 857.
22. G. E. Backus, J. F. Gilbert, Uniqueness in the inversion of inaccurate gross earth data. *Philos. Trans. R. Soc. London* **Series A 266,** 123–192 (1970).
23. P. J. Goodwin, N. F. Boyd, Mammographic parenchymal pattern and breast cancer risk: a critical appraisal of the evidence. *Am. J. Epidemiol.* **127,** 1097–1108 (1988).
24. M. B. McSweeney, W. C. Small, V. Cerny, W. Sewell, R. W. Powell, J. H. Goldstein, Magnetic resonance imaging in the diagnosis of breast disease: use of transverse relaxation times. *Radiology* **153,** 741–744 (1984).
25. C. S. Poon, M. J. Bronskill, R. M. Henkelman, N. F. Boyd, Quantitative magnetic resonance parameters and their relationship to mammographic pattern. *J. Natl. Cancer Inst.* **84,** 777–781 (1992).

(43.) Graham S., Stanchev P., Bronskill M., "Criteria for Analysis of Multicomponent Tissue T_2 Relaxation Data", ***MRM***, No 35, 1996, 370-378.